

Effects of an Equatorial "Wall" on an Atmospheric Model

K. MIYAKODA AND L. UMSCHIED, JR.—Geophysical Fluid Dynamics Laboratory, NOAA, Princeton, N.J.

ABSTRACT—The effect of an artificial lateral boundary (the wall) at the Equator on a simulated atmospheric circulation was studied numerically. By comparing the solutions of two 30-day integrations of a global model with and without the wall, we found that the discrepancies of the wind and temperature at the middle and high latitudes became appreciable at approximately 8 days and serious at approximately 12 days. This suggests that the wall (hemispheric) model may be applied as a forecast model for a maximum of about 12 days. The disagreement in the wind between the two cases starts just below the tropo-

pause level at the Equator and spreads toward the higher latitudes. Eventually, the middle latitudes respond to this equatorial effect, and the disagreement is amplified to the natural variability level. Insertion of the wall considerably increases the condensation of water vapor in the Tropics for the winter hemisphere; the reverse is true for the summer hemisphere. The result is that, in the winter hemisphere, the tropical troposphere and the stratosphere are cooler and the higher latitude troposphere is warmer in the wall case than in the control case. The opposite is true for the summer hemisphere.

1. INTRODUCTION

If the domain of a prediction model is truncated artificially, errors start to grow from the boundary, spread, and distort the overall solutions. Then, what is the time range of the validity of the solutions for the limited domain model? This paper is concerned with discussing the limitation on the *hemispheric model*—how quickly and in what way does the wall (equatorial boundary in the hemispheric model) influence the solutions in the middle latitudes.

Baumhefner (1971, 1972), using the six-layer model of the National Center for Atmospheric Research, investigated this problem and concluded that the wall at the Equator did not appreciably influence the forecast in the middle latitudes for nearly 2 weeks. Miyakoda et al. (1971) also tried to answer this question, but the results were inconclusive because of an inherent weakness in the model and the inadequate approach used; nevertheless, some advantages of the global prediction were recognized. The present study is an extension of Baumhefner's work. The study is worthwhile and perhaps necessary to answer some unsolved questions.

The cumulative forecast results with the hemispheric model of the Geophysical Fluid Dynamics Laboratory (GFDL) revealed that the practical limit of predictability of flow fields is 10 days for January cases and a little longer for those in July (Miyakoda et al. 1972). Why is the time so short when compared with the ultimate limit of predictability of about 3 weeks? (For the GFDL model, see Smagorinsky 1969.) There are, of course, a number of possible factors to determine this time range. Here, however, we consider only the equatorial wall effect. We have evidence that the wall creates a serious distortion in the solution starting on the 12th day of prediction.

The problem of the wall effect also relates directly or indirectly to other problems such as the lateral coupling

of disturbances between the Tropics and the middle and high latitudes, the tropical wind data requirement in four-dimensional analysis, and the telecommunication effect of the equatorial sea-surface temperature anomaly on the middle-latitude cyclones and anticyclones.

Regarding the interaction between the Tropics and higher latitudes, theoretical studies have been made in connection with the search for the energy source for the Tropics. Although a fairly good picture now has been obtained, the past effort has been focused mostly on studying the conditions under which the wave energy from the middle latitudes can penetrate into the Tropics (e.g., Charney 1969, Mak 1969, and Bennett and Young 1971). The question of how quickly and to what extent the disturbance propagates outward from the Tropics to middle latitudes has not been discussed. There is, however, a study that touched upon the problem in numerical experiments, although it was not primarily addressed to this specific question. In the study of tropical wind data requirements, Gordon et al. (1972), found that the flow and the mass fields are poorly balanced at the Equator and, as a result, the analysis error appears to be a maximum at the Equator just below the tropical tropopause and extends even to middle latitudes.

2. ATMOSPHERIC MODEL AND EXPERIMENT

The model is a nine-level general circulation model on the modified Kurihara grid. In the model, the number of grid points are increased zonally (especially near the poles) in comparison with the original Kurihara grid. The horizontal resolution is $N=24$, meaning that 24 equally spaced rows of gridpoints are distributed from the Equator to the pole with a spacing of 417 km or 3.75° . It is exactly the same model used previously in the simulation experiments for determining wind data requirements in the Tropics (Gordon et al. 1972).

A long-range integration of the equations was carried out in the same way as normally done in the numerical simulation of the general circulation of the global atmosphere. The position of the Sun is for January; thus the solutions correspond to those of a perpetual January (not the January in the marching season). The solutions, therefore, are somewhat unrealistic but perhaps acceptable for the present study.

For comparison, we selected an arbitrary period from the total span of the general circulation simulation and repeated the integration for 1 mo with the wall model. The original run is now regarded as the control, and the results in the modified run are called wall solutions. The wall model is produced by placing a wall at the Equator in the global model. The wall is physically a rigid, free-slip, and insulated boundary that prohibits the exchange of momentum, heat, and moisture not only between the hemispheres but also between one hemisphere and the equatorial wall itself.

Relevant to the above conditions are eq (1) through (6):

$$\frac{\partial(p_s u)}{\partial t} + \dots + \frac{\partial(p_s v u \cos \theta)}{a \cos \theta \partial \theta} + \dots = \frac{\partial \tau_{\lambda \theta}}{a \partial \theta}, \quad (1)$$

$$\frac{\partial(p_s v)}{\partial t} + \dots + \frac{\partial(p_s v v \cos \theta)}{a \cos \theta \partial \theta} + \dots = \frac{\partial \tau_{\theta \theta}}{a \partial \theta}, \quad (2)$$

$$\frac{\partial(p_s T)}{\partial t} + \dots + \frac{\partial(p_s v T \cos \theta)}{a \cos \theta \partial \theta} + \dots = \frac{\partial H_\theta}{a \partial \theta}, \quad (3)$$

$$\frac{\partial(p_s q)}{\partial t} + \dots + \frac{\partial(p_s v q \cos \theta)}{a \cos \theta \partial \theta} + \dots = \frac{\partial E_\theta}{a \partial \theta}, \quad (4)$$

$$\frac{\partial p_s}{\partial t} = \int_0^1 \left[\frac{\partial(p_s u)}{a \cos \theta \partial \lambda} + \frac{\partial(p_s v \cos \theta)}{a \cos \theta \partial \theta} \right] d\sigma, \quad (5)$$

and

$$\omega = -p_s \sigma \left(\frac{\partial \dot{\sigma}}{\partial \sigma} - \frac{\dot{\sigma}}{\sigma} + \nabla \cdot \mathbf{V} \right) \quad (6)$$

where t is time, λ is longitude, θ is latitude, σ is the vertical sigma coordinate, p_s is surface pressure, u and v are respectively the zonal and meridional components of the wind vector, T is the temperature, q is the mixing ratio of water vapor to dry air, $\tau_{\lambda \theta}$ and $\tau_{\theta \theta}$ are the two elements of the Reynolds stress tensor, and H_θ and E_θ are respectively the heat and the moisture transfer by subgrid scale turbulence. The equatorial boundary conditions in the wall model at $\theta=0$ are

$$\begin{aligned} v &= 0, \\ \tau_{\lambda \theta} &= \tau_{\theta \theta} = 0, \\ H_\theta &= 0, \end{aligned}$$

and

$$E_\theta = 0.$$

In practice, the equations are not treated at the equatorial gridpoints; at the gridpoints next to the equatorial

points, the poleward fluxes in the second terms on the left side of eq (1) through (4) and the stresses and transfers in terms on the right side of these equations are set to zero. In eq (5), the pressure tendency equation, and eq (6), the omega equation, v is set to zero at the lateral boundaries facing the Equator.

In the wall run, the initial conditions were taken from the control run, and the prediction calculation was started using Euler-backward time differencing for a quarter of a day (to control the gravity wave) and then was continued with centered differencing.

3. GROWTH AND PROPAGATION OF DISCREPANCIES

Our main concern is the differences between the solutions for the wall run and the control run, which are called discrepancies or sometimes called errors in this paper.

First, let us define the discrepancy; for example, the temperature discrepancy is given by

$$\Delta T = T_{wall} - T_{contr}$$

where T_{wall} and T_{contr} are the temperatures in the wall and control runs, respectively. The square of the discrepancy is sometimes vertically averaged; thus

$$\frac{\int_{surf}^{\infty} \rho (\Delta T)^2 dz}{\int \rho dz} = \frac{\int_{p_s}^0 (\Delta T)^2 dp}{\int dp} = \overline{(\Delta T)^2}^p$$

where the integration with respect to z is performed from the ground surface to infinity. It is converted to the pressure integral from the surface pressure p_s to zero where $\overline{(\quad)}^p$ means the vertical average.

$$\frac{\sum_i m_{i,j} (\Delta T)^2}{\sum_i m_{i,j}} = \overline{(\Delta T)^2}^\lambda$$

or

$$\frac{\sum_{i,j} m_{i,j} (\Delta T)^2}{\sum_{i,j} m_{i,j}} = \overline{(\Delta T)^2}^{\lambda \theta}$$

where i and j are respectively indexes of the grid for λ and θ directions, $m_{i,j}$ is the horizontal area of the grid box (i,j) , $\overline{(\quad)}^\lambda$ is the zonal average, and $\overline{(\quad)}^{\lambda \theta}$ is the horizontal average.

Overall Growth

The measures used to gage the overall growth of discrepancies are the root mean square (rms) error of wind and temperature averaged vertically and horizontally. There are two horizontal domains of averaging, one is the

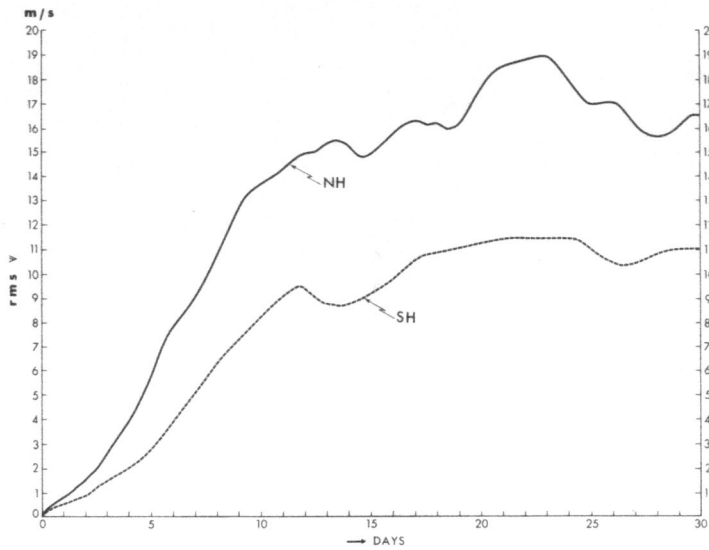


FIGURE 1.—The rms discrepancies of wind.

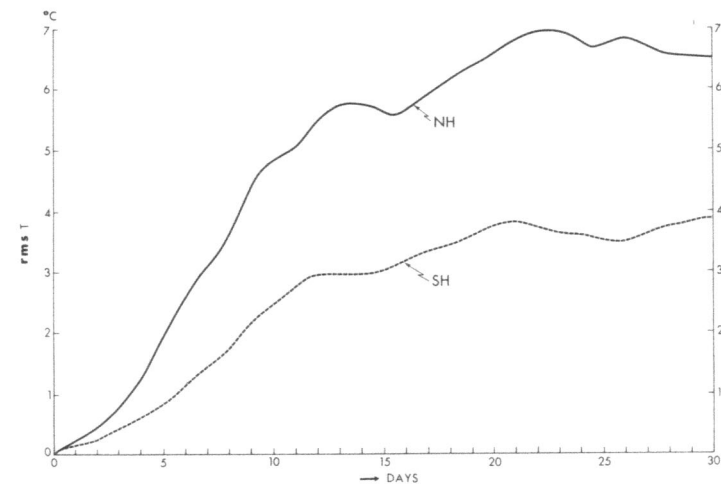


FIGURE 2.—The rms discrepancies of temperature.

Northern Hemisphere north of 15°N (NH) and the other the Southern Hemisphere south of 15°S (SH).

The developments of the wind error,

$$\sqrt{\frac{(\Delta u)^2 + (\Delta v)^2}{2^p}}^{\lambda \theta}$$

and the temperature error,

$$\sqrt{\frac{(\Delta T)^2}{2^p}}^{\lambda \theta}$$

are respectively shown in figures 1 and 2.

Both figures indicate that the discrepancies grow distinctly but gradually with time. Since it is winter in the Northern Hemisphere and summer in the Southern Hemisphere during January, the discrepancies are larger in NH than in SH. In all cases, the growth rates are high until about 12 days; and after about 20 days, the errors seem to fluctuate around their asymptotic values. Baumhefner (1971) did *not* find large differences between the wall run and control at 12 days.

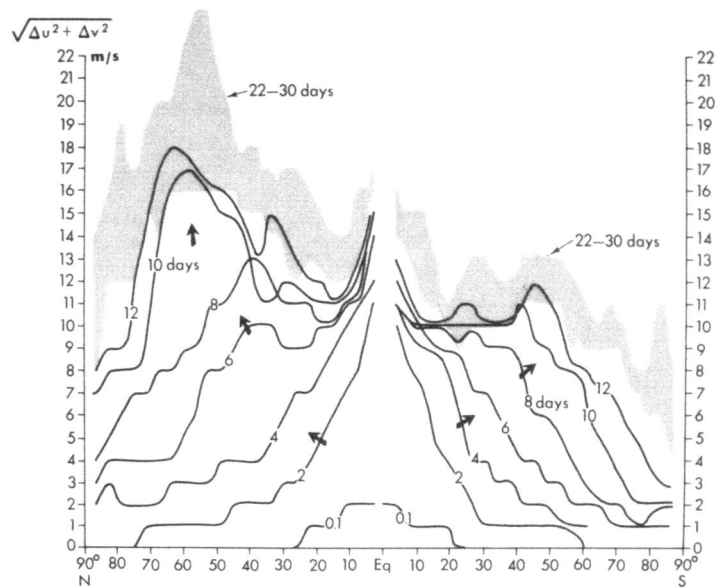


FIGURE 3.—Latitudinal propagation of wind difference.

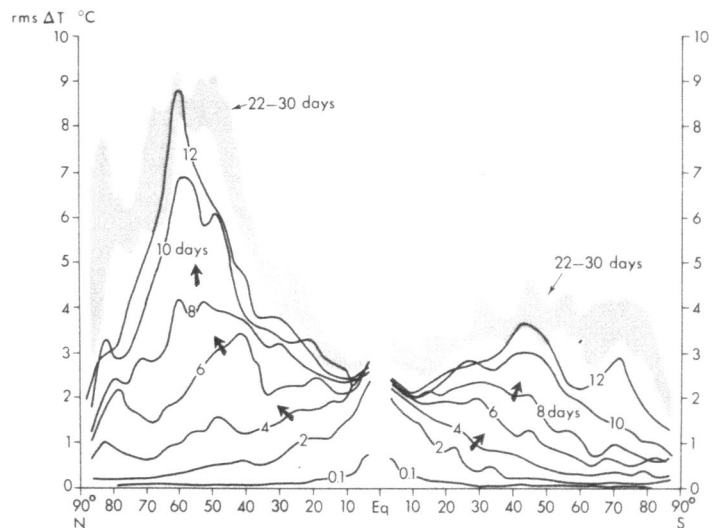


FIGURE 4.—Latitudinal propagation of temperature difference.

Note that the development of the discrepancy is much faster than in earlier predictability experiments (Smagorinsky 1969) in which the initial temperature errors are given randomly with a magnitude of 0.5°C in rms. Thus, the similarity of two forecasts with slightly different initial conditions is still recognizable at the end of 2 weeks, whereas the solutions of the wall run turn out to be substantially altered from those of the control run at 12 days.

Meridional Propagation

To see the horizontal propagation of the discrepancies, we present in figures 3 and 4 the latitudinal distributions of errors given by

$$\sqrt{\frac{(\Delta u)^2 + (\Delta v)^2}{2^p}}^{\lambda}$$

and

$$\sqrt{\frac{(\Delta T)^2}{2^p}}^{\lambda}$$

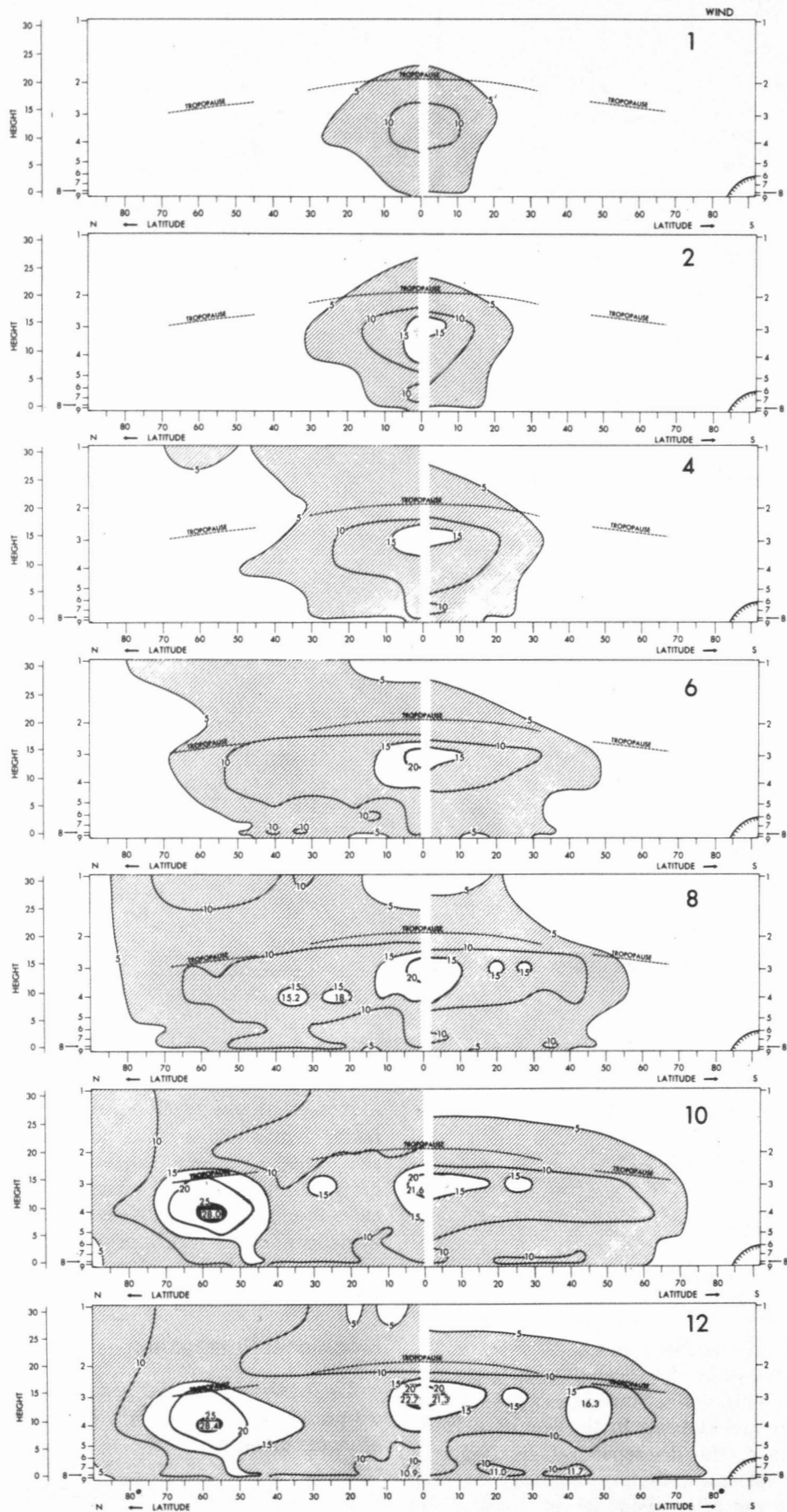


FIGURE 5.—Propagation of wind discrepancy (m/s) in a meridional section. The ordinate is the vertical height (km).

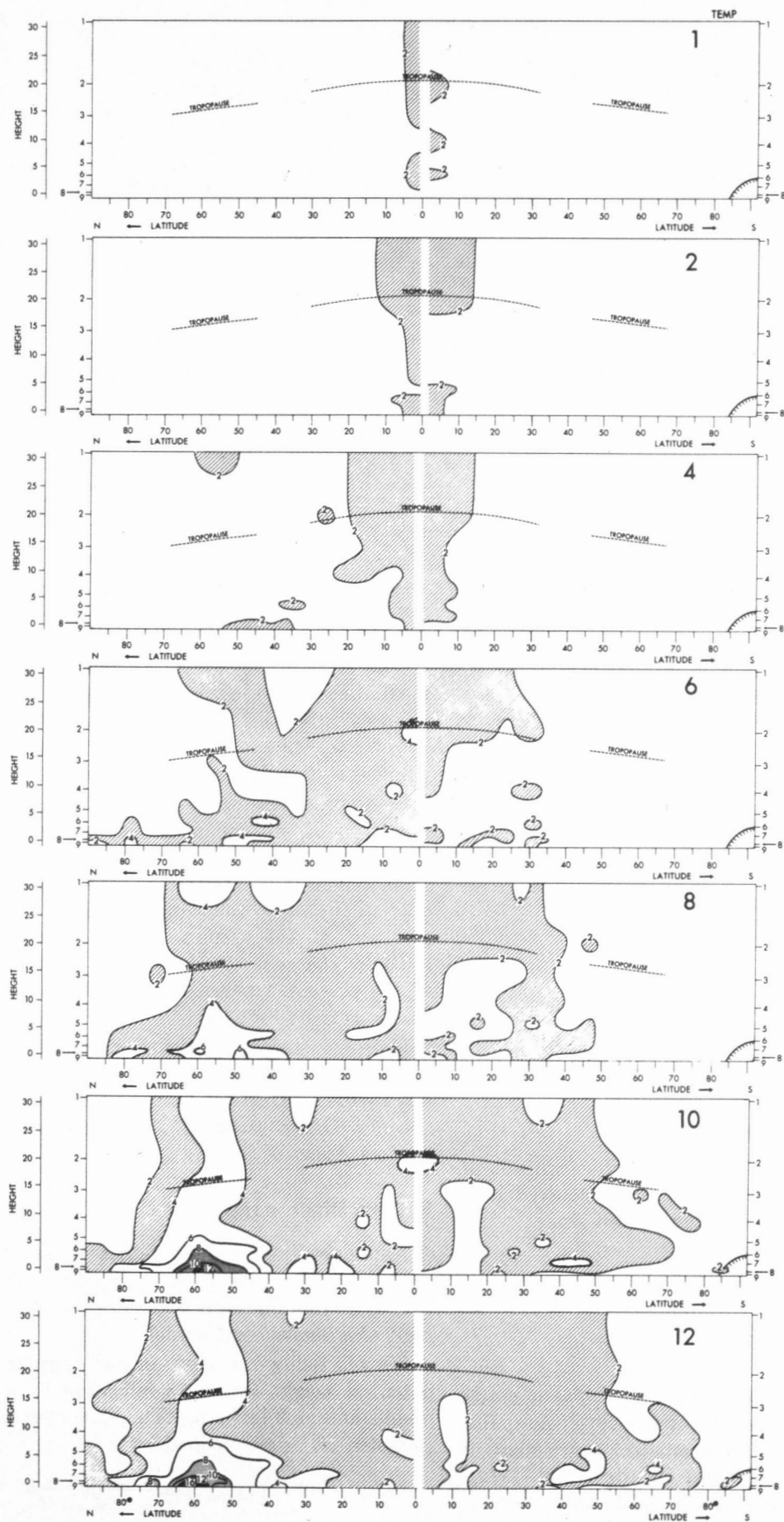


FIGURE 6.—Propagation of temperature discrepancy ($^{\circ}\text{C}$) in a meridional section. The ordinate is the vertical height (km).

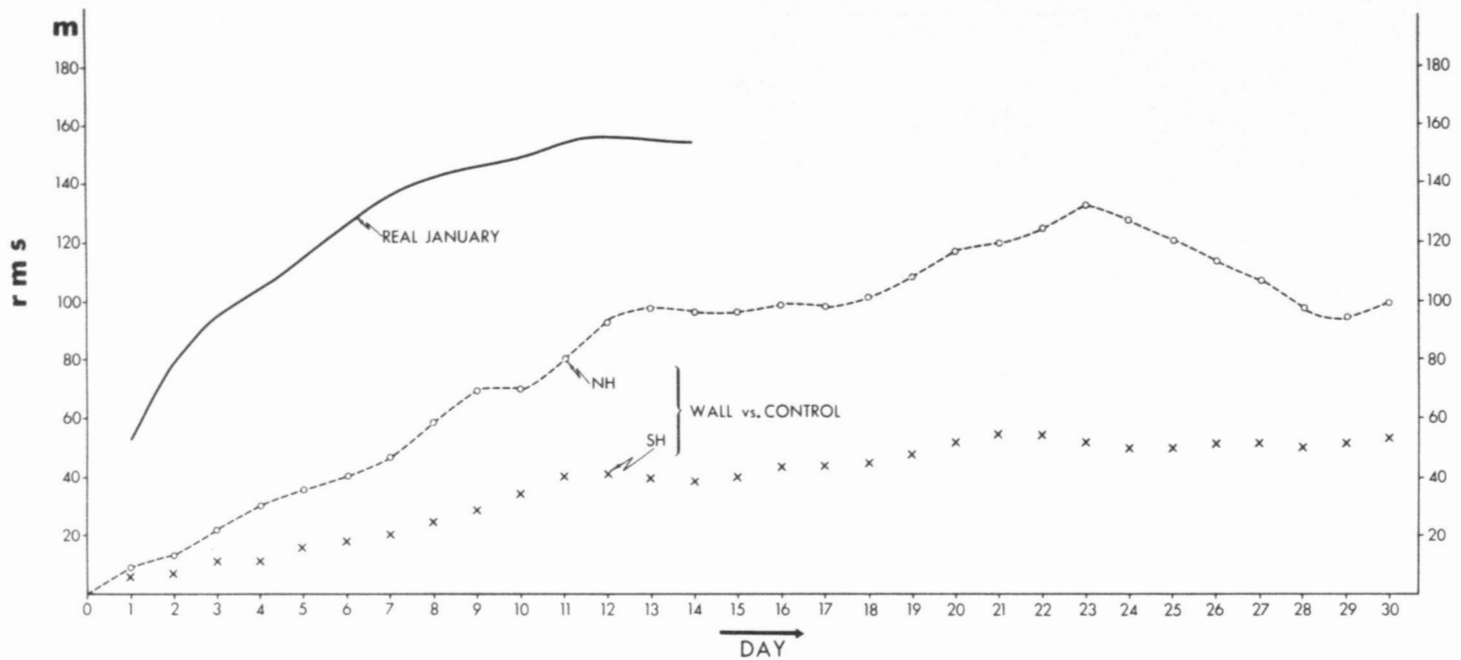


FIGURE 7.—The rms discrepancies of 500-mb geopotential height. The solid line depicts the rms error of 2-week real forecasts with the GFDL 1967 version model.

The errors start at the Equator and propagate toward the higher latitudes. The figures include the error curves for 0.1, 2, 4, 6, 8, and 12 days. The shaded area is given as a reference; it is the envelope of the discrepancy curves for the period from day 22 to 30. The errors fluctuate within the shaded area after they reach the saturation level and presumably will not grow much beyond this level.

From these figures, we see that, by the 8th day, the discrepancies have grown to a sizable magnitude in the middle and high latitudes; on the 12th day, they reach the asymptotic levels. The discrepancies reach a higher magnitude in the middle latitudes primarily due to the middle-latitude baroclinicity.

In the analysis of error development, Irvine and Houghton (1971) noted that "the error tends to move toward the core of maximum velocity." This is reasonable and is in agreement with our case.

Propagation in a Meridional Section

Figures 5 and 6 show another aspect of the evolution of discrepancies for wind and temperature. Displayed in a height-latitude section, the variables treated are

$$\sqrt{(\Delta u)^2 + (\Delta v)^2}^{\lambda}$$

and

$$\sqrt{(\Delta T)^2}^{\lambda}$$

From figure 5, it is clear that the wind discrepancy starts at the Equator just below the tropopause level. A similar feature was also noticed in the numerical experiment of the tropical wind data requirement (Gordon et al. 1972), although in their case the discrepancy is the analysis error that resulted from data assimilation with a prediction model. The mechanism, however, is presumably common to both cases.

The layer of maximum discrepancy is just below the maximum eddy kinetic energy at the Equator (fig. 11). Subsequently, the discrepancies extend poleward at the upper tropospheric layer, and then the middle latitudes respond to this discrepancy. (See day 10 in fig. 5.)

Relating to the wave energy propagation, whether or not tropical disturbances can propagate outside the Tropics has been controversial. Kasahara and Williamson (1972) claim that "the tropics are shielded in one direction only in the sense that information in the tropics barely gets out of the tropics, but information in the mid-latitudes can penetrate into the tropics. . . ." The results of the present experiment, however, do not conform to this picture.

Figure 6 shows the development of the temperature discrepancy. It appears first in the equatorial stratosphere; but in the end, the discrepancy at the middle latitudes becomes larger. In particular, there are large values in the lower part of the troposphere.

Pattern Discrepancy

Note how quickly the similarity of the two flow patterns deteriorates because of the wall effect. This information will be useful and important for ascertaining the ultimate limit of a hemispheric model.

We will follow the conventional approach of using geopotential height for the verification of forecasts at the middle and high latitudes. The first score is the rms of the geopotential height defined by

$$\text{rms} = \sqrt{(Z_{\text{wall}} - Z_{\text{contr}})^2}^{\lambda\theta}$$

The second score is the correlation coefficient (correl coeff) for the deviation of the geopotential height from the tem-

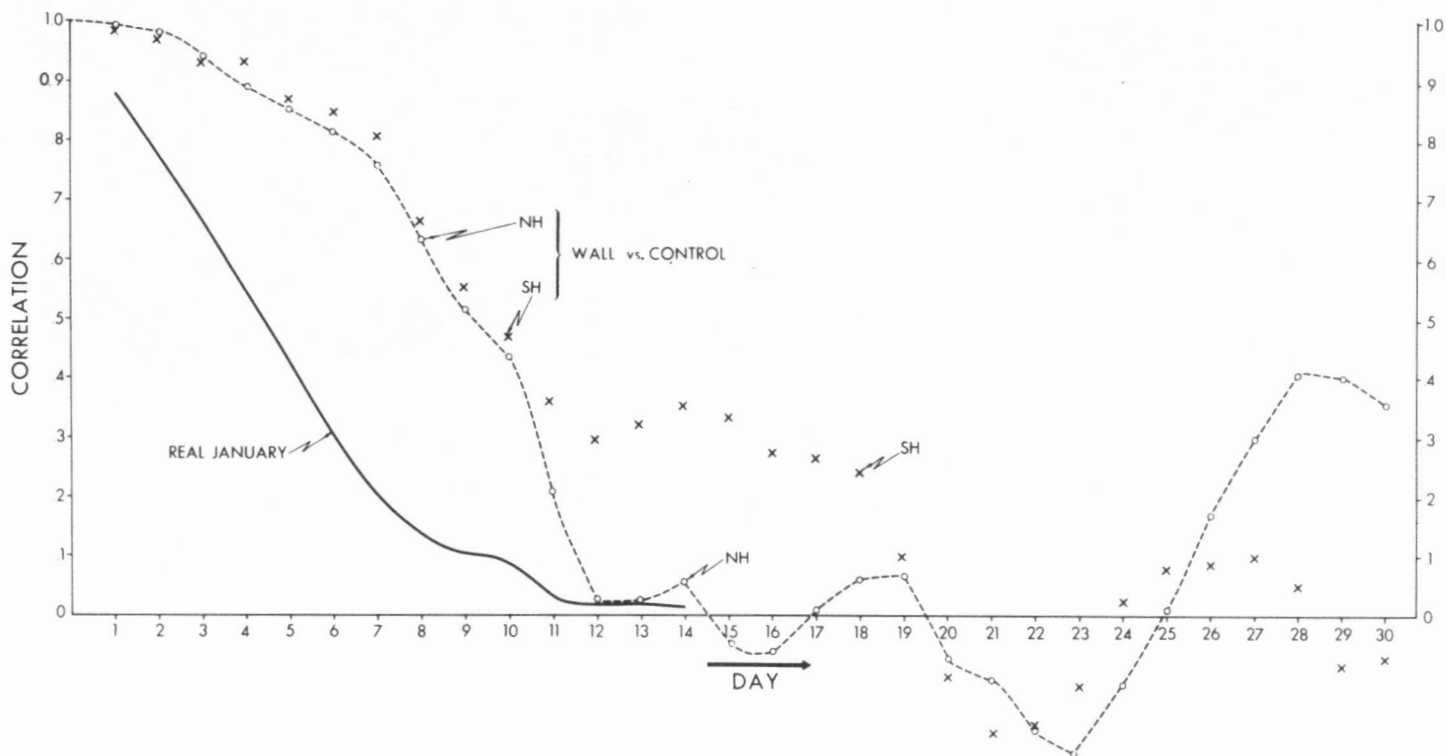


FIGURE 8.—Correlation coefficient of 500-mb height anomalies. The solid line shows the coefficient curve of 2-week real forecasts.

poral average. For this purpose, we first define the deviation (or anomaly); thus

$$\delta Z_{contr} = Z_{contr} - Z_{averg}$$

and

$$\delta Z_{wall} = Z_{wall} - Z_{averg}.$$

In the above formulas, Z_{averg} is the time average for the period from 21 to 30 days. Introducing

$$\delta Z'_{contr} = \delta Z_{contr} - \overline{\delta Z_{contr}}^{\lambda\theta}$$

and

$$\delta Z'_{wall} = \delta Z_{wall} - \overline{\delta Z_{wall}}^{\lambda\theta},$$

we then obtain

$$\text{correl coeff} = \frac{\overline{(\delta Z'_{contr})(\delta Z'_{wall})}^{\lambda\theta}}{\sqrt{[\overline{(\delta Z'_{contr})^2}]^{\lambda\theta} [\overline{(\delta Z'_{wall})^2}]^{\lambda\theta}}}$$

Figures 7 and 8 include these scores for the geopotential height at the 500-mb level only. The circles and crosses are the values for NH and SH, respectively. The general features of the time evolution of rms in figure 7 are similar to those of wind and temperature in figures 1 and 2. In figure 7, the ensemble average rms error of the 500-mb height field based upon real forecasts for 12 January cases is also shown as a reference. The real forecasts were made for 2-week periods with a GFDL hemispheric model (the 1967 version) and compared with observations (Miyakoda et al. 1972). The magnitude of the error for the real January cases is much higher than the magnitude of the discrepancy marked by NH in the present study because

the present global model has a systematic bias in the intensity of disturbances as a result of poor horizontal grid resolution and excessive viscous dissipation.

Figure 8 shows the correlation coefficients for the deviation of geopotential heights at the 500-mb level. The circles and crosses are the results in the present experiment. This is only one sample; however, if many samples were included, these values would probably show a narrow range of variation at the beginning but would have a wide fluctuation after the mean value reached the zero line. It is important to note in figure 8 that the correlation coefficients start to drop rapidly at 7 days, approach zero, and then fluctuate after 12 days in the NH and somewhat later in the SH. This indicates that the anomaly components of the two patterns have no resemblance whatever after 12 days.

In the same figure, the ensemble mean of the correlation coefficients based upon the 12 January cases of real forecasts is shown for reference. Inspecting this figure, one may be led to conclude that (1) the wall determines a limit of forecasts (i.e., 12 days in winter and a little longer in summer) and (2) the score of real forecasts for the first 6 days is far below the NH curve in the present experiment. This suggests that there is room for improvement within the framework of the hemispheric model. On the other hand, so far as the limit of predictability in general is concerned, it is envisaged that the removal of the wall may provide a possibility to increase the time range beyond 10 days.

A question may arise as to why the summer (SH) forecast has skill for a longer period than the winter (NH) forecast. This may be explained by the fact that,

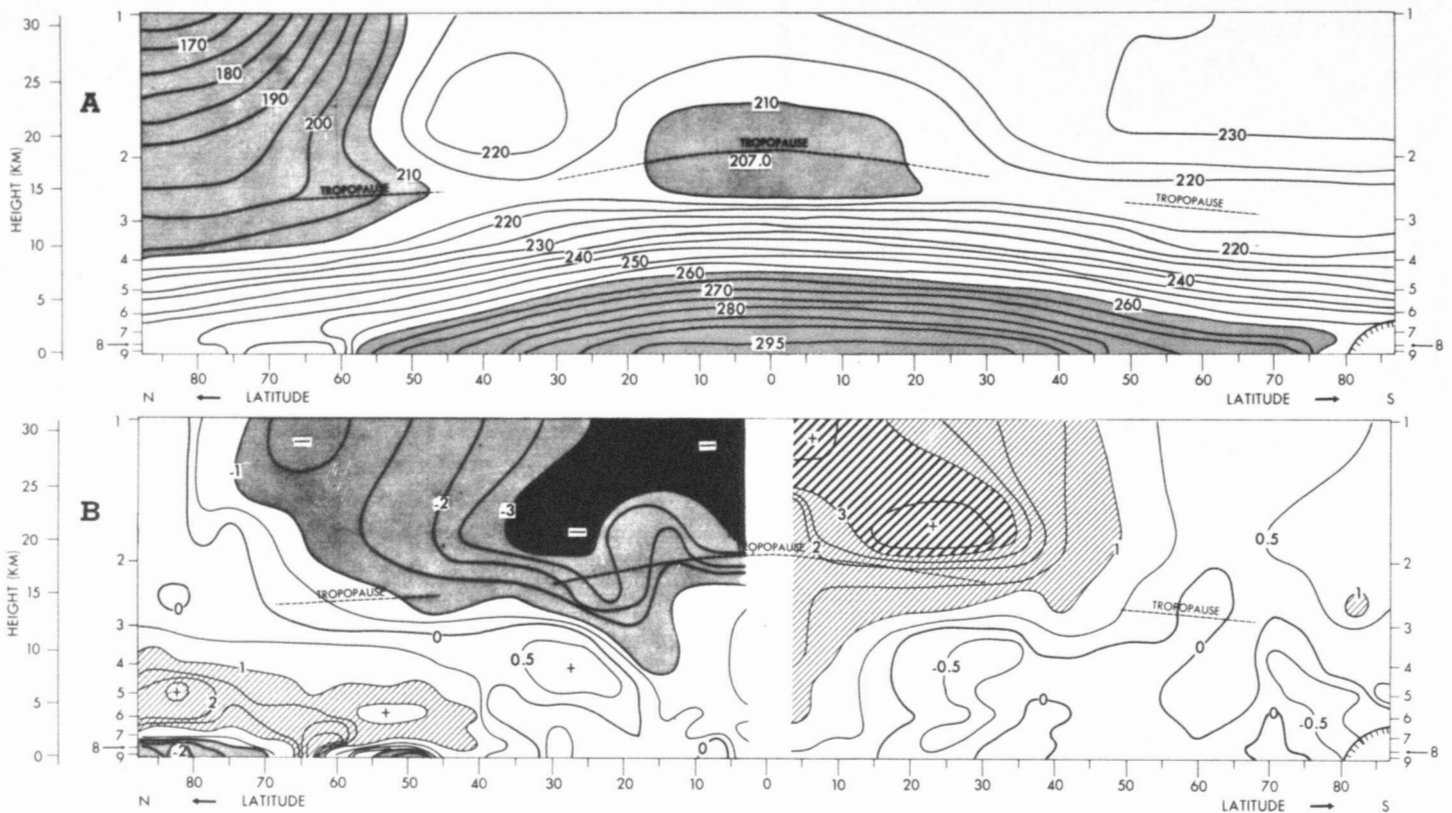


FIGURE 9.—(A) temperature ($^{\circ}\text{K}$) for the control case and (B) discrepancy (i.e., the wall minus the control case). The ordinate is the vertical height (km). In (B), values greater than 1 are hatched and those less than -1 are shaded.

in the summer hemisphere, the distortion of the Hadley circulation is less severe than in the winter hemisphere. Baumhefner (1971) made an interesting experiment in this connection; he studied the effect of the wall by placing it at various latitudes. Significant damage was observed in the Northern Hemisphere in less than a week when the wall was inserted at 10°N or 20°N .

4. DISCREPANCIES IN THE TEMPORAL AND ZONAL MEANS

To have an overall impression of the wall effect on the general circulation, we calculated the zonal averages of variables and the discrepancies. Here we show only selected variables that may be of special interest. This type of averaging was already partially treated by Miyakoda et al. (1971) and Baumhefner (1972), although the averaging period is different. The period in this study is from 10 to 30 days; whereas Miyakoda et al. (1971) adopted a period of 4 to 14 days, and Baumhefner's (1972) case is for day 7. There are several common features in the results shown below and the previous works, but there are disagreements also.

Temperature

The meridional section of temperature for the control run is exhibited in figure 9A. The meridional section of temperature for the wall run is similar to this; therefore, only the discrepancy is displayed in figure 9B. The magni-

tude of the temperature difference is sizable, and the distribution of the discrepancy is systematic. For the wall run in the Northern Hemisphere, the stratosphere as well as the tropical troposphere is cooler; the troposphere in the higher latitudes (except in the surface boundary layer) is warmer. In the Southern Hemisphere, the opposite is true.

Zonal Wind

Figure 10 shows the zonally averaged zonal wind for the control and the wall runs. There are two salient aspects of this figure. One is that the stratospheric easterlies at the Equator are weaker in the wall case (fig. 10B) than in the control (fig. 10A); the difference, however, is not as appreciable as in the case of Miyakoda et al. (1971). Second, the latitudinal position of the subtropical jet in the Northern Hemisphere is shifted poleward in the presence of the wall; the shift is about 10° in latitude. The similar tendency was also pointed out by Baumhefner (1971), but for the case of the wall at 10°N or 20°N , not for the case at the Equator.

Eddy Kinetic Energy

The eddy kinetic energy is defined here as

$$K_E = \frac{1}{2} (u'^2 + v'^2)$$

where u' and v' are the eddy components of wind vectors

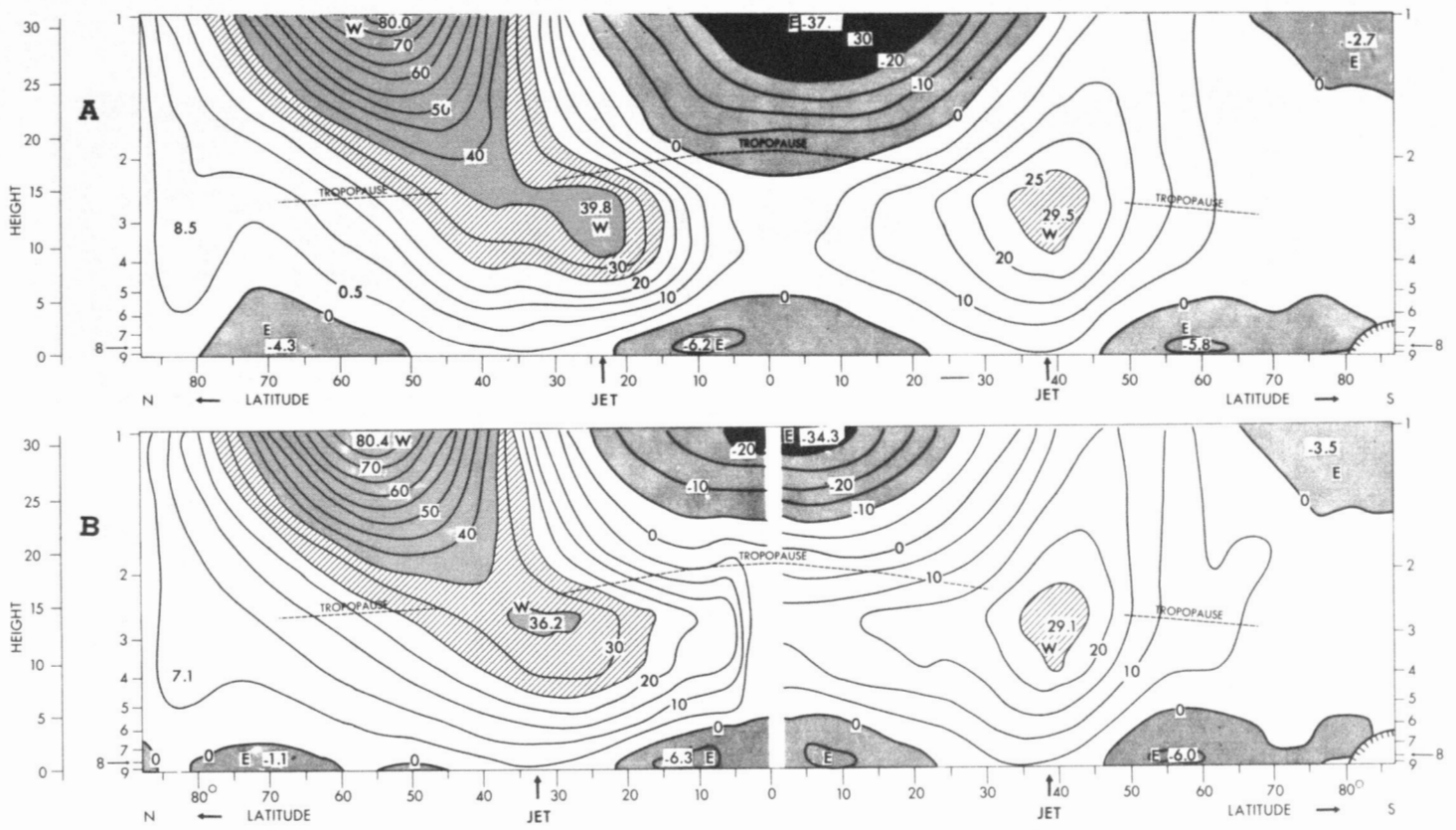


FIGURE 10.—Zonal wind (m/s) for (A) the control case and (B) the wall case. The W's are westerlies; the E's are easterlies (negative values). The latitudinal positions of the jet streams are indicated by arrows. The ordinate is the vertical height (km).

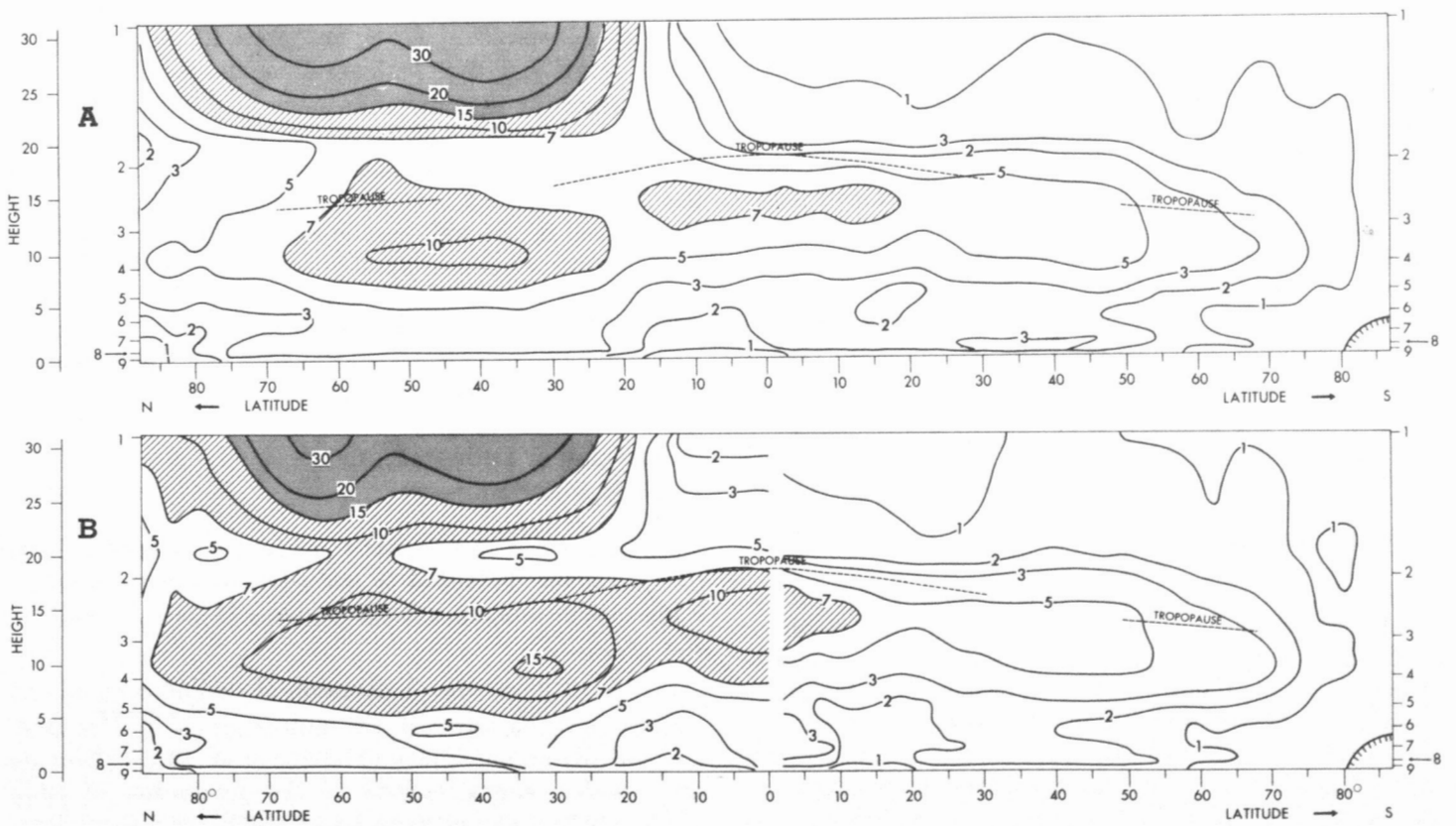


FIGURE 11.—Eddy kinetic energy ($10^5 \text{ cm}^2 \text{ s}^{-2}$) for (A) the control case and (B) the wall case. Included are hatched areas (intensity greater than $7 \times 10^5 \text{ cm}^2 \text{ s}^{-2}$) and shaded areas (intensity greater than $15 \times 10^5 \text{ cm}^2 \text{ s}^{-2}$). The ordinate is the vertical height (km).

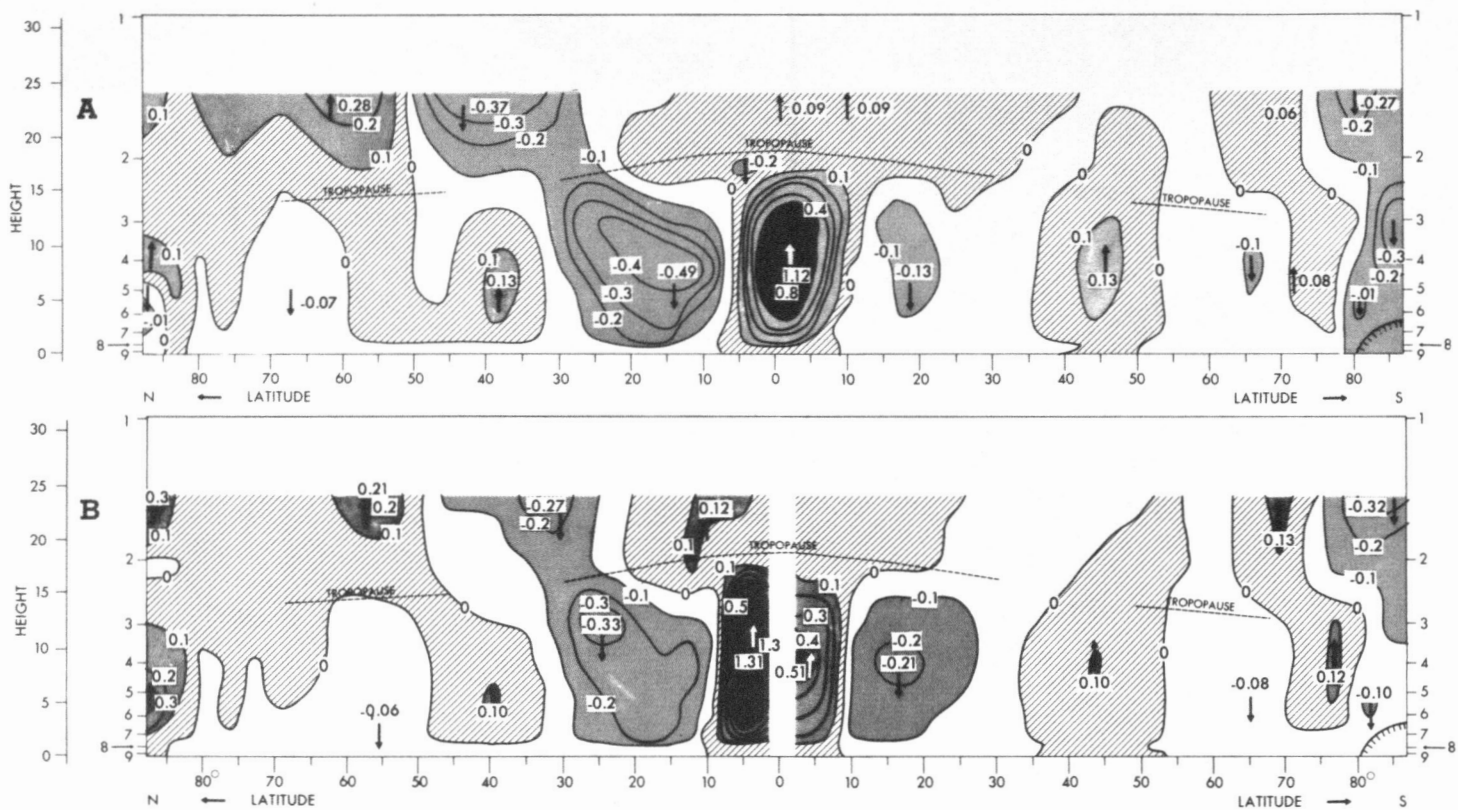


FIGURE 12.—Vertical velocity (cm/s) for (A) the control case and (B) the wall case. The hatched areas have values between 0.0 and 0.1; the lightly shaded areas, less than -0.1 ; and the heavily shaded areas, greater than 0.5. The ordinate is the vertical height (km).

(i.e., $u' = u - \bar{u}^\lambda$ and $v' = v - \bar{v}^\lambda$). The air density is not included in this definition of eddy kinetic energy. The meridional section of this variable is shown in figure 11. It can be seen that the intensities are apparently considerably less than reality. The intensities both at the middle latitudes and at the Equator are markedly larger for the Northern Hemisphere in the wall case than the other; they are almost the same for the Southern Hemisphere. The fact that the eddy kinetic energy at the Equator is greater in the presence of wall is one of the most intriguing results in this experiment. The increased eddy kinetic energy at the Equator is because of the effect of liberated heat of condensation along the wall. According to Hayashi (1973), the waves containing the energy in the wall case would be mostly stationary waves and partly westward-moving Rossby-type waves (Matsuno 1966 and Rosenthal 1965) with the maximum u component over the Equator.

Vertical Velocity

Figure 12 is the vertical velocity distribution. It indicates the structure of the tropospheric and stratospheric meridional circulation. In the control run, the well-known three-cell circulations in the troposphere are dominant both in the Northern and Southern Hemispheres, and the Ferrel cells are present in both hemispheres. The peculiar downward current near the equatorial tropopause [reported in Miyakoda et al. (1971)] is recognized only slightly this time. The existence of a strong downward flow over the Antarctic Plateau clearly deserves more

attention. Note also that, in the winter stratosphere, a downward current associated with the polar-night jet is typically observed at 50°N ; in figure 12, however, it is closer to 40°N . This is because of the model's bias.

Look next at the difference between the two runs. The tropical upward current in the troposphere is located at about 4°S in the control case; with the wall, the center of the upward current is located right at the Equator. The Hadley cell in the wall case is intersected in the middle; thereby, the cell is considerably intensified in the NH but is weakened in the SH. It is noteworthy that the Ferrel cells in the middle latitudes are noticeably weaker in both hemispheres in the wall run, although the dynamical significance is presently not clear.

Conversion of Eddy Potential To Eddy Kinetic Energy

The term $\overline{\omega'\alpha'}$ represents the rate of conversion from eddy available potential to eddy kinetic energy where α is the specific volume, ω is the pressure velocity, $\omega' = \omega - \bar{\omega}^\lambda$, and $\alpha' = \alpha - \bar{\alpha}^\lambda$.

Figure 13 shows the distribution of the intensity of this term; in practice, however, the term $(c_p/g) \overline{(p_s \delta)'} T'$ is used. As generally accepted now (Manabe et al. 1970), there are three major source regions of the generation of eddy kinetic energy; two of them are at about the 600-mb level in middle latitudes of both the Northern and Southern Hemispheres, and the third is at the 300-mb level in

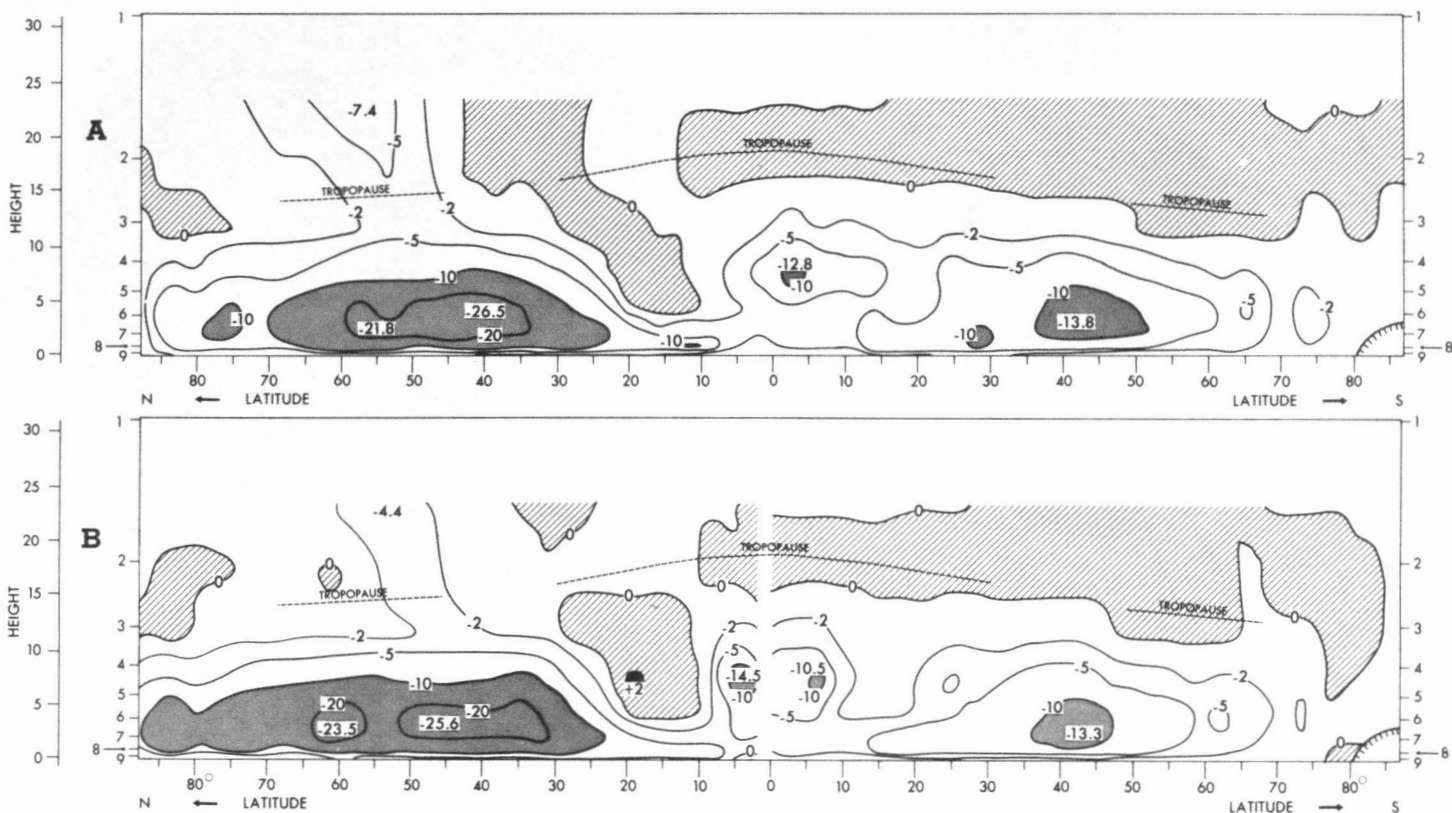


FIGURE 13.—Rate of conversion ($10^3\text{g}\cdot\text{s}^{-3}$) between eddy available potential and eddy kinetic energy, $(c_p/g)(p_s\sigma)'\overline{T'}$, for (A) the control case and (B) the wall case. The ordinate is the vertical height (km).

equatorial regions. Turning to the wall effect, we see in figure 13B that the generation for the middle latitudes in the Northern Hemisphere is not greater in the wall run. On the other hand, the generation near the Equator is intensified for the Northern Hemisphere and slightly decreased for the Southern Hemisphere. It is of special interest that the energy transformation at the Equator is increased by the presence of the wall. This fact is consistent with the increase of the eddy kinetic energy at the Equator, suggesting that the equatorial kinetic energy is well controlled by generation in situ.

Precipitation and Evaporation

Figure 14A gives the latitudinal distribution of the daily rate of precipitation; figure 14B gives the distribution of evaporation. In the control run, the peak of rainfall is located at about 4°S ; in the wall run, it is right at the Equator. For the wall run, the rate of precipitation appears higher in the Northern Hemisphere and lower in the Southern Hemisphere. This indicates that, normally, a large amount of water vapor is carried from the Northern Hemisphere toward the Southern Hemisphere in January, but water vapor is trapped by the barrier at the Equator; as a result, rain in the wall model appears greater in the Northern Hemisphere and smaller in the Southern Hemisphere than in the control run. This feature was previously pointed out by Miyakoda et al. (1971), although the case was for March and the mean declination of the sun was only 4°S .

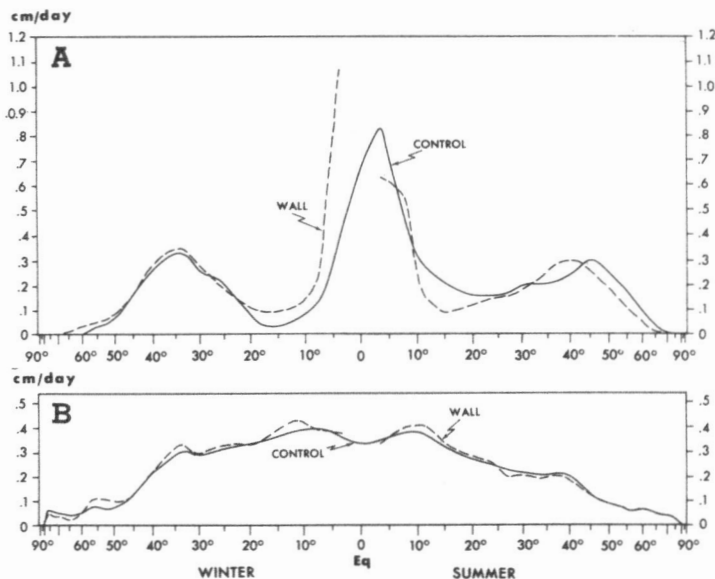


FIGURE 14.—Daily rate of (A) precipitation and (B) evaporation.

Discussion

Summarizing the results described above, we now try to construct a consistent physical picture of the wall effect. The effect is tentatively divided into two parts—direct and indirect.

The direct effects are the following. First, the Hadley circulation cell in the troposphere is intersected by the wall; thereby, the position of the upward current is

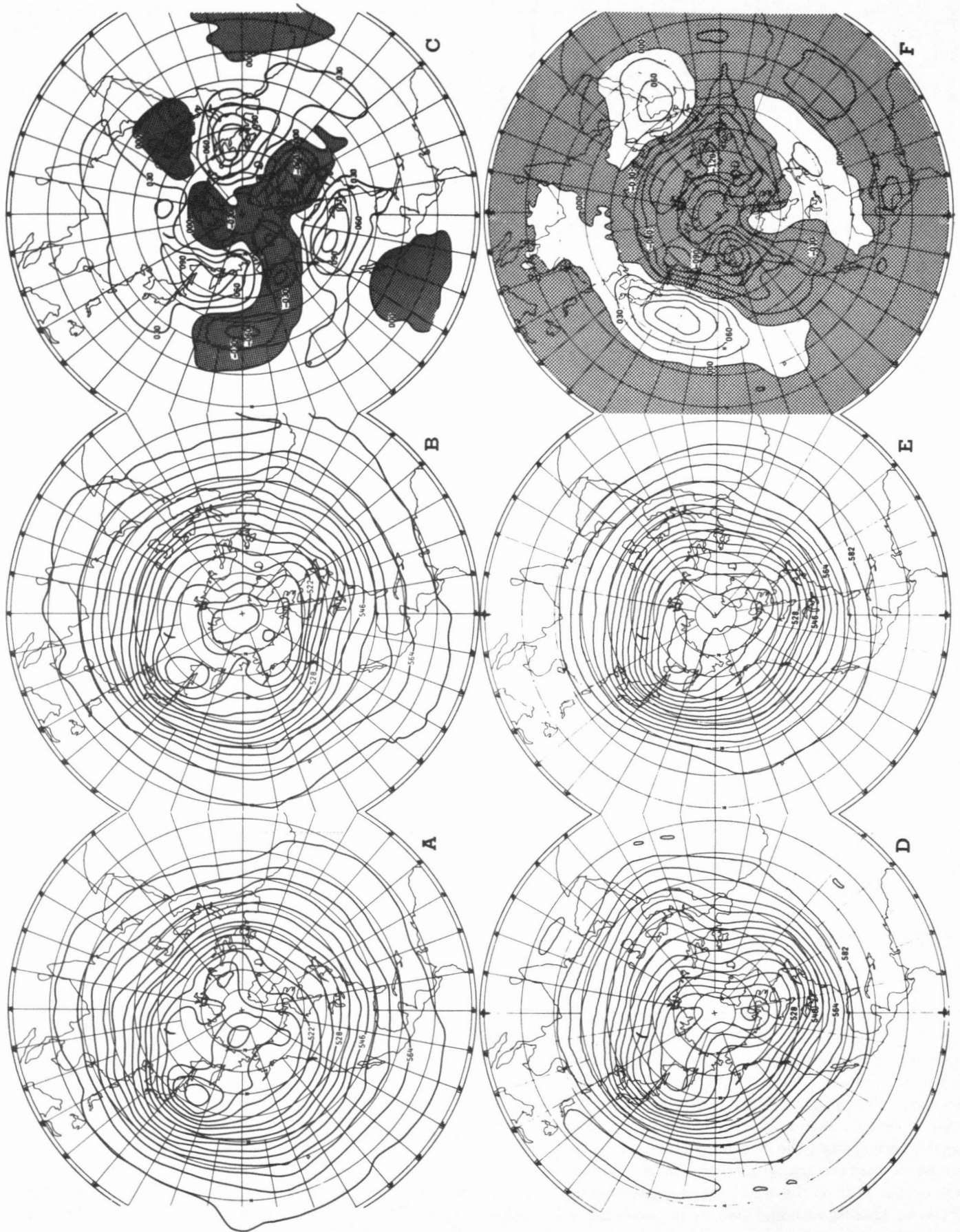


FIGURE 15.—The 500-mb geopotential heights for (A) the control case, (B) the wall case, and (C) the discrepancy [i.e., (B)–(A)]. The observation (D), the prediction (E), and the error (F) [i.e., (E)–(D)] are needed for comparison.

shifted from the summer hemisphere to a position right at the Equator. Second, in the presence of the wall, the stratospheric easterlies in the Tropics are weakened because of the lack of the cross-equatorial current (fig. 10). This is readily understandable in terms of angular momentum transfer.

The indirect effects were first brought about by the shift of the upward current position of the Hadley cell as well as the prohibition of the cross-equatorial transport of moisture and heat. The rate of rainfall in the Tropics is increased for the Northern Hemisphere and decreased for the Southern Hemisphere (fig. 14). Consistent with the change in the liberation of condensation heat, the upward current at the wall becomes appreciably stronger for the Northern Hemisphere and weaker for the Southern Hemisphere (fig. 12). Then, the downward current region of the Hadley circulation is shifted northward in both hemispheres.

These effects in turn bring about the further changes. Accompanied by the latitudinal shift of the Hadley cell and also by the change in the meridional transfer of momentum, the position of the subtropical jet at the 200-mb level is displaced poleward in the Northern Hemisphere (fig. 10). [Baumhefner (1971) found that the poleward shift of the jet axis is very drastic (about 15° latitude) if the wall is inserted at 20°N.] As a consequence of the change in the upward current in the Tropics, the stratosphere and the tropical troposphere in the Northern Hemisphere appear to be colder because of the adiabatic cooling while the opposite is true in the Southern Hemisphere (fig. 9). On the other hand, in the middle- and high-latitude troposphere, the temperature is higher in the Northern Hemisphere in the wall model; again, the opposite is true in the Southern Hemisphere. The processes taking place are not simple. They are the mixture of two effects—namely, the adiabatic warming because of the intense downward current of the Hadley cell (in the middle latitude) and the intense meridional transfer of heat by eddies (in the lower layers in the high latitudes).

5. IMPACT ON THE TROUGHS AND RIDGES IN MIDDLE LATITUDES

The discussion now proceeds to a somewhat detailed aspect—that is, the effect on the structure of the extratropical disturbances. We are, however, still not concerned with the very small-scale disturbances but only with the stationary or slowly moving troughs and ridges in the middle latitudes.

Figure 15 exhibits the time mean of geopotential heights on a stereographic projection at the 500-mb level for the Northern Hemisphere. This represents the planetary scale flow fields in the middle and high latitudes. Figures 15A through 15C represent the present experiments; figures 15D through 15F are taken from the collective results of the real forecasts with the GFDL hemispheric model that treated 12 January cases (Miyakoda et al. 1972).

Figures 15D through 15F represent reality and are shown for comparison. Figures 15A and 15B are the time-averaged fields for the period from 10 to 30 days for the control and the wall runs, respectively. Figure 15C is the difference of the two fields (i.e., wall minus control). Figures 15D and 15E are the means of 12 winter samples for the period 4 to 14 days for the observed and the forecasts. Figure 15F is the difference (i.e., the prediction minus the observation).

Look first at figures 15A and 15B. Since this is one sample, it is likely that the solution does not coincide well with the model's climatology. Yet, one may see roughly the dominating mode (i.e., the zonal wave number 3), the major troughs at 140°E and 70°W, and a minor trough at 40°E in both the control and wall maps. These features roughly correspond to reality, with a slight shift of the zonal position (See figs. 15D and 15E.)

We now are concerned with whether or not the equatorial wall effect may give an explanation to the systematic bias of the height fields in real forecasts with the hemispheric model. To see this, we compare figures 15C and 15F. The characteristic features in the discrepancy map are the three pairs of positive and negative regions along the 50°–60° latitude band. This shows that the troughs in the wall run are systematically shifted eastward compared with those in the control run. The agreement, however, of the discrepancy maps (figs. 15C and 15F) is hardly discernible, indicating that the error in the real forecasts (fig. 15F) cannot be explained by the wall effect alone.

6. CONCLUSIONS

The wall erected at the Equator in a global model produces the following effects.

1. The wind and temperature at the middle latitudes are modified appreciably at 8 days and seriously at 12 days.

2. The wind difference first appears just below the equatorial tropopause level and then extends to the middle latitudes. The temperature difference also starts at the Equator; then, the middle latitudes respond to the equatorial disturbances. Eventually, the temperature difference is largest in the lower troposphere in middle latitudes.

3. In the zonal mean distribution, the effects are the following. The temperature receives a systematic influence such that the stratosphere and tropical troposphere for the winter hemisphere become cooler and the troposphere at high latitudes becomes warmer; the tendency is the opposite for the summer hemisphere. The subtropical jet for the winter hemisphere is displaced poleward by about 10° latitude. The equatorial stratospheric easterlies appear considerably weaker. Rain in the Tropics is intensified for the winter hemisphere and is weakened for the summer hemisphere. The Hadley cell is intersected by the wall; thereby, the winter hemispheric part is considerably intensified, and the summer hemispheric part is weakened.

The eddy kinetic energy is substantially increased for the winter hemisphere but not for the summer hemisphere.

4. The presence of the wall causes a systematic and appreciable eastward shift of the position of the troughs and ridges for the large-scale flows at the middle latitudes.

5. In view of the wall effects described above (particularly because of conclusion 1), it is not surprising that a practical forecast with a hemispheric model has no skill beyond 10 days for winter and slightly later for summer.

Some criticisms, however, of the present experiment do exist; for example, only one sample is included, and the model has relatively poor horizontal and vertical grid resolution. The second defect may be related to a third defect, a bias in the distribution of the zonal wind at the equatorial region; for example, the westerlies extend to the Equator (fig. 10). Since the vertical shear is an important factor in the instability and the structure of tropical waves (Yamasaki 1969, Holton 1971, and Murakami 1972), the model might have a serious bias in the generation and propagation characteristics of the disturbances in the equatorial region.

ACKNOWLEDGMENTS

The authors thank J. Smagorinsky, Y. Hayashi, C. T. Gordon, and J. R. Holton for important suggestions. D. H. Lee, D. G. Hembree, and T. Mauk provided valuable assistance. The authors also thank Betty Williams for typing the manuscript.

REFERENCES

- Baumhefner, David P., "On the Effects of an Imposed Southern Boundary on Numerical Weather Prediction in the Northern Hemisphere," *Journal of the Atmospheric Sciences*, Vol. 28, No. 1, Jan. 1971, pp. 42-54.
- Baumhefner, David P., "Further Experimentation with an Imposed Southern Boundary for Large-scale Numerical Weather Prediction," *Journal of the Atmospheric Sciences*, Vol. 29, No. 4, May 1972, pp. 768-772.
- Bennett, John R., and Young, John A., "The Influence of Latitudinal Wind Shear Upon Large-scale Wave Propagation Into the Tropics," *Monthly Weather Review*, Vol. 99, No. 3, Mar. 1971, pp. 202-214.
- Charney, Jule G., "A Further Note on Large-scale Motions in the Tropics," *Journal of the Atmospheric Sciences*, Vol. 26, No. 1, Jan. 1969, pp. 182-185.
- Gordon, C. T., Umscheid, L. Jr., and Miyakoda, K., "Simulation Experiments for Determining Wind Data Requirements in the Tropics," *Journal of the Atmospheric Sciences*, Vol. 29, No. 6, Sept. 1972, pp. 1064-1075.
- Hayashi, Y., "Spectral Analysis of Tropical Disturbances Appearing in a GFDL General Circulation Model," 1973 (to be published).
- Holton, James R., "A Diagnostic Model for Equatorial Wave Disturbances: The Role of Vertical Shear of the Mean Zonal Wind," *Journal of the Atmospheric Sciences*, Vol. 28, No. 1, Jan. 1971, pp. 55-64.
- Irvine, William S., Jr., and Houghton, David D., "Propagation of Systematic Errors in a One Layer Primitive-equation Model for Synoptic Scale Motion," *Monthly Weather Review*, Vol. 99, No. 8, Aug. 1971, pp. 606-616.
- Kasahara, A., and Williamson, D., "Evaluation of Tropical Wind and Reference Pressure Measurements. Numerical Experiments for Observing Systems," *Tellus*, Vol. 24, No. 2, 1972, pp. 100-115.
- Mak, Man Kin, "Laterally Driven Stochastic Motions in the Tropics," *Journal of the Atmospheric Sciences*, Vol. 26, No. 1, Jan 1969, pp. 41-64.
- Manabe, Sykuro, Holloway, J. Leith Jr., and Stone, Hugh M., "Tropical Circulation in a Time-integration of a Global Model of the Atmosphere," *Journal of the Atmospheric Sciences*, Vol. 27, No. 4, July 1970, pp. 580-613.
- Matsuno, Taroh, "Quasi-geostrophic Motions in the Equatorial Area," *Journal of the Meteorological Society of Japan*, Ser. 2, Vol. 44, No. 1, Feb. 1966, pp. 25-42.
- Miyakoda, K., Moyer, R. W., Stambler, H., Clarke, R. H., and Strickler, R. F., "A Prediction Experiment With a Global Model in the Kurihara Grid," *Journal of the Meteorological Society of Japan*, Vol. 49 (special issue), Dec. 1971, pp. 521-536.
- Miyakoda, K., Hembree, G. D., Strickler, R. F., and Shulman, I., "Cumulative Results of Extended Forecast Experiments. I. Model Performance for Winter Cases," *Monthly Weather Review*, Vol. 100, No. 12, Dec. 1972, pp. 836-855.
- Murakami, Takio, "Equatorial Tropospheric Waves Induced by Diabatic Heat Sources," *Journal of the Atmospheric Sciences*, Vol. 29, No. 5, July 1972, pp. 827-836.
- Rosenthal, Stanley L., "Some Preliminary Theoretical Considerations of Tropospheric Wave Motions in Equatorial Latitudes," *Monthly Weather Review*, Vol. 93, No. 10, Oct. 1965, pp. 605-612.
- Smagorinsky, J., "Problems and Promises of Deterministic Extended Range Forecasting," *Bulletin of the American Meteorological Society*, Vol. 50, No. 5, May 1969, pp. 286-311.
- Yamasaki, M., "Large-scale Disturbances in the Conditionally Unstable Atmosphere in Low Latitudes," *Papers in Meteorology and Geophysics*, Vol. 20, No. 4, Meteorological Research Institute, Tokyo, Japan, 1969, pp. 289-336.

[Received February 8, 1973; revised July 3, 1973]